-

LME-MPM applied to quasi-brittle fracture.

Miguel Molinos[a1], Pedro Navas[a2], Diego Manzanal[a], and Manuel Pastor[a]

[a] *ETSI Caminos, Canales y Puertos, Universidad Politéctnica de Madrid.*
c. Prof. Aranguren 3, 28040 Madrid, Spain

Abstract

The objective of this work is to introduce an alternative technique to address the fracture process of brittle and quasi-brittle materials under the Material Point Method (MPM) framework. With this purpose the eigensoftening algorithm, developed originally for the Optimal Transportation Meshfree (OTM) approximation scheme, is extended to the MPM with the aim of presenting a suitable alternative to the existing fracture algorithms developed for the MPM. The good fitting in the predictions made by the eigensoftening algorithm against both analytical and experimental results proofs the well performance of the method when challenging applications are to modeled.

Keywords: Quasi brittle fracture, Local-*Max-Ent* approximation, Material Point Method, Solid Dynamics

1. Introduction

The presence of cracks is a violation of the continuity requirement of the Finite Element Method (FEM). To overcome this issue, numerous numerical artifacts have been proposed with the aim of reproducing such a complex behaviour. These techniques vary from the employment of cohesive approaches [1, 2], to the gradual insertion of cohesive elements [3, 4, 5] at solid elements boundaries, or handling arbitrary crack paths by level set representation of the fracture surface [6]. The simulation of fracture propagation in a more accurate and effective way can be considered as one of the ongoing goals of the development of novel spatial discretization methods like meshfree techniques. Some examples of it are the Material Point Method (MPM) [7, 8, 9, 10], the Element-Free Galerkin Method (EFGM) [11, 12, 13, 14], the Smoothed Particle Hydrodynamics (SPH) [15, 16], the

---

[1]Corresponding author: m.molinos@alumnos.upm.es
[2]Corresponding author: p.navas@upm.es

Optimal Transportation Meshfree (OTM) [17, 18, 19, 20] or Peridynamics [21, 22] among others.

Regarding MPM, fracture has been treated numerically through two different ways . On the one hand, the "CRAcks with Material Points (CRAMP)" is proposed [9, 23]. The basis of this methodology consist of the removal of the restriction of the single-valued velocity field close to the crack through, at least, two sets of nodes. In this method, different labels are assigned to the material points and nodes to distinguish if they are in the same side of the crack or not. Under this approach, crack surface is described with line segments in 2D and triangle patches in 3D cases. The chosen criteria for crack propagation is based on such parameters as energy release rate analyzed by Tan & Nairn (2002)[24], and the stress intensity factor or the J-integral discussed by Guo & Nairn (2004)[25]. On the other hand, the foundation of the second approach is the introduction of failed material points to describe the crack evolution. In these methods, the formation of failed points describes the nucleation of cracks, and thereafter its propagation and branching. Consequently, the position of the crack does not need to be explicitly stated. This fact represents significant advantages over the "CRAMP". Under this approach, the prediction of failure evolution is computed with a decohesion model, which has been discussed by Chen *et al.*[10] and Schreyer *et al.*[7]. Successful simulations are provided within the framework of the fracture of brittle materials by Chen *et al.* [8, 26] and Sulsky & Schreyer [27].

Similar to this approach, Schmidt *et al.* [28] introduced the concept of eigenfracture, where crack sets are approximated by means of eigen-deformations, which enable the material to develop displacement jumps at no cost of local elastic energy. Later, the eigenerosion approach to brittle facture was carried out by Pandolfi *et al.* [29, 19]. In this technique, the concept of "erosion" of the material point is depicted, being the material point able to remain intact or become completely failed or eroded, when no loading capacity is bore . This method has been successfully applied to simulate high complex phenomena such as dynamic fragmentation of metals [20]. Recently, Zhang *et al.* [30] adopted the eigenerosion to resolve the dynamic fracture of brittle materials in the MPM framework. Nonetheless, when quasi-brittle materials are simulated though this approach, the results exhibit an overestimation of tensile stress and strain peaks. Furthermore, since the work of Zhang *et al.* [30] is made with conventional MPM/GIMP, stress oscillations are to be faced.

To overcome the limitations observed in the EigenMPM [30], the present

3

research proposes the eigensoftening algorithm developed by Navas *et al.* [31, 32] for the OTM framework and engineered for quasi-brittle materials. Inspired in the concept of the crack band model [33], since energy dissipation is performed through the softened (or failed) volume, this methodology is able to capture the gradual rather than abrupt dissipation of the fracture energy. Moreover, in order to mitigate stress oscillations as well as to deal with tensile instabilities, such those that occurs when particles crosses an element boundary, the work of Molinos *et al.* [34] is followed. The traditional MPM technique is enhanced through the Local Maximum-Entropy (LME) approximation technique [35] for the spatial discretization as well as a explicitly MPM Newmark Predictor-Corrector (NPC) scheme is derived for the time discretization.

The paper is structured as follows. First meshfree methodology, eigenerosion and eigensoftening algorithms are presented in Section 2. Then, both approaches are compared and verified by means of comparisons with analytical and experimental results in Section 3. Finally, relevant conclusions are exposed in Section 4.

2. The meshfree methodology

The aim of this section is to describe and introduce some special techniques required to face the fracture problem under the MPM framework. In consequence, this section is structured as follows: first, in 2.1, the Newmark Predictor-Corrector (NPC) algorithm for the MPM will be exposed; next the LME approximants are introduced in 2.2 as an accurate alternative technique to interpolate data between particles and nodes, and finally fracture algorithms based on the eigendeformation concept are presented in 2.3.

2.1. The MPM time integration : A Newmark Predictor-Corrector scheme

The MPM [36] is a meshfree Lagrangian-Eulerian method where moving material points, henceforth in this research, particles ($\square_p$) will carry on all the physical information of the local state (σ_p, ε_p) and a set of fixed background nodes ($\square_I$) will be introduced to compute the balance of momentum equation. Since the MPM possesses the advantages of both Lagrangian and Eulerian descriptions, no element distortion takes place in the MPM. Therefore, it is an appropriate and efficient method to solve problems with moving discontinuities such as fracture evolution.

Without loosing generality, the MPM algorithm can be described with three main steps: (i) a variational recovery process, where particle data is projected to the grid nodes, (ii) an Eulerian step, where balance of momentum

4

equation is expressed as a nodal equilibrium equation in a FEM-like procedure, and finally (iii) a Lagrangian advection of the particles. In the present research, an explicit predictor-corrector time integration scheme is adopted. The purpose of this choice is motivated due to its proved robustness and stability for dynamic computations. In the first stage, the nodal velocity predictor $\vec{\tilde{v}}_I^{k+1}$ is computed through nodal velocities $\vec{v}_I$ and accelerations $\vec{a}_I$ and evaluated in the k time step,

$$\vec{\tilde{v}}_I^{k+1} = \frac{N_{Ip}^k m_p (\vec{v}_p^k + (1-\gamma)\,\Delta t\,\vec{a}_p^k)}{\mathbf{m}_I^{k+1}} \; . \tag{1}$$

Where γ is an user-defined parameter (typically adopted as 0.5), $\mathbf{m}_I$ represents the lumped mass matrix, and N_{Ip}^k is the nodal contribution of the shape function evaluated in the particle coordinates $\vec{x}_p^k$. This way of computing the nodal predictor is numerically stable as well as minimises the computational effort. Once nodal velocities are obtained, the essential boundary conditions are imposed. After that, an Eulerian phase is computed in the set of nodes in a FEM-like way, where nodal forces $\vec{f}_I^{k+1}$ are computed through the equilibrium equation. Next the nodal velocities are corrected in a *corrector* stage:

$$\vec{v}_I^{k+1} = \vec{v}_I^{pred} + \gamma\,\Delta t\,\frac{\vec{f}_I^{k+1}}{\mathbf{m}_I^{k+1}} \; . \tag{2}$$

Finally, in order to update the particles, those are advected in the Lagrangian stage as

$$\vec{a}_p^{k+1} = \frac{N_{Ip}^k \vec{f}_I^k}{\mathbf{m}_I^k} \; , \tag{3}$$

$$\vec{v}_p^{k+1} = \vec{v}_p^n + \Delta t\,\frac{N_{Ip}^k \vec{f}_I^k}{\mathbf{m}_I^k} \; , \tag{4}$$

$$\vec{x}_p^{k+1} = \vec{x}_p^n + \Delta t\,N_{Ip}^k\,\vec{v}_I^k + \frac{1}{2}\Delta t^2\,\frac{N_{Ip}^k \vec{f}_I^k}{\mathbf{m}_I^k} \; . \tag{5}$$

The complete pseudo-algorithm it is summarised in Appendix A.

2.2. Spatial interpolation technique : Local Maximum-Entropy approximants

Local Maximum-Entropy (LME) approximation scheme was introduced by Arroyo & Ortiz (2006)[35] as a bridge between finite elements and meshfree methods. The key idea under this interpolation technique is the interpretation of each nodal value N_I as a probability. Related with this definition,

two important limits are introduced. First the maximum-entropy (*max-ent*) limit, which ensures a *unbiased statistical inference* based on the nodal data as states the Jayne's[37] principle of *maximum entropy*. And second the Delaunay triangulation that warranties the *least width* shape function support. To reach to a compromise between two competing objectives, a Pareto set is defined as,

$$(\text{LME})_\beta \text{ For fixed } \vec{x} \text{ minimise } f_\beta(\vec{x}_p, N_I) := \beta U(\vec{x}_p, N_I) - H(N_I)$$

$$\text{subject to } \begin{cases} N_I \geq 0, \ I=1, \ ..., \ n \\ \sum\limits_{I=1}^{N_n} N_I = 1 \\ \sum\limits_{I=1}^{N_n} N_I \vec{x}_I = \vec{x} \end{cases}$$

where $H(N_I)$ is the entropy of the system of nodes following the definition given by Shannon (1948) [38], the shape function width is defined as $U(\vec{x}_p, N_I) := \sum_I N_I |\vec{x}_p - \vec{x}_I|^2$, and β is a regularization o *thermalization* parameter such that for Pareto optimal solutions $\beta \in (0, \infty)$. Notice that β has units of $[L]^{-2}$, therefore it can be controlled by adjusting a dimensionless parameter[3], $\widehat{\gamma} = \beta h^2$, where h is defined as a suitable measure of the nodal spacing. With the restrictions of the Pareto set, the unique solution of the local *max-ent* problem LME_β is,

$$N_I^*(\vec{x}) = \frac{\exp\left[-\beta \ |\vec{x} - \vec{x}_I|^2 + \vec{\lambda}^* \cdot (\vec{x} - \vec{x}_I)\right]}{Z(\vec{x}, \vec{\lambda}^*)}, \tag{6}$$

where $Z(\vec{x}, \vec{\lambda}^*)$ is the *partition function* defined as,

$$Z(\vec{x}, \vec{\lambda}) = \sum_{I=1}^{N_n} \exp\left[-\beta \ |\vec{x} - \vec{x}_I|^2 + \vec{\lambda} \cdot (\vec{x} - \vec{x}_I)\right], \tag{7}$$

and a Lagrange multiplier $\vec{\lambda}^*$ such minimise the function $\log Z(\vec{x}, \vec{\lambda})$. The traditional way to compute the optimal value of $\vec{\lambda}^*$ is through a Newton-Raphson procedure, or in more challenging scenarios by a combination of the Newton-Raphson and the Nelder-Mead Simplex algorithms [32]. Nonetheless, since

---

[3]To avoid confusion with the γ parameter of the NPC, the dimensionless parameter defined in Arroyo & Ortiz [35] as γ will be represent by $\widehat{\gamma}$ to preserve as much as possible the original notation.

finite strains are not involved in the present research, Newton-Raphson is an enough efficient method. For an uniform nodal spacing, β can be considered constant, thus first derivatives of the interpolation technique ∇N_I^* can be obtained by evaluating the following expression

$$\nabla N_I^* = -N_I^* \left(\mathbf{J}^*\right)^{-1} \left(\vec{x} - \vec{x}_I\right) \tag{8}$$

where $\mathbf{J}$ is the Hessian matrix, defined by

$$\mathbf{J}(\vec{x}, \vec{\lambda}, \beta) \equiv \frac{\partial \vec{r}}{\partial \vec{\lambda}}, \tag{9}$$

$$\vec{r}(\vec{x}, \vec{\lambda}, \beta) \equiv \frac{\partial \log Z(\vec{x}, \vec{\lambda})}{\partial \vec{\lambda}} = \sum_I^{N_n} p_I(\vec{x}, \vec{\lambda}, \beta) \left(\vec{x} - \vec{x}_I\right). \tag{10}$$

An additional remark concerning the support of the interpolation function is that, in practice, the value of N_I decay exponentially following $\exp(-\beta\vec{r})$. In this sense, a good practice is to truncate it under a tolerance (typically around 10^{-6}) that would ensure a reasonable range of neighbours, see [35] for details. This tolerance defines a limit value of the influence radius to find the neighbour nodes of a given integration point.

2.3. Fracture modelling approach

Within the context of MPM formulation, fracture can be modelled by failing particles according to a suitable failure criterion. When material points are failed, they are assumed to have null stress tensor. To reproduce this behaviour in the present research, the eigensoftening algorithm is introduced in the MPM framework as an alternative approach to the decohesion model [10, 7]. The eigensoftening concept was originally developed by Navas *et al.* (2017)[31] as an extension for quasi-brittle materials of the eigenerosion proposed by Pandolfi & Ortiz (2012)[29] for fracture of brittle materials. A comparison between both in [31] shows that the eigenerosion algorithm significantly overestimates the tensile stress and the strain peaks, meanwhile eigensoftening captures the forces and crack patterns accurately. On the other hand, eigensoftening algorithm agrees very well with experimental results in all the aspects. Furthermore, the accuracy of this algorithm has been proven for complex fracture patterns such as the ones obtained with fiber reinforces concrete (FRC), [39].

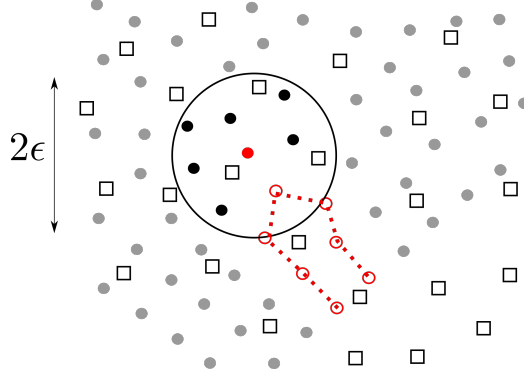The key idea behind the eigenerosion algorithm is the computation of the

Figure 1: Scheme of a linear cohesive law, where the shaded area is G_f, f_t is the tensile strength, and w_c is the critical opening displacement.

energy-release rate attendant to the failure of material point p,

$$G_p^{k+1} = \frac{C_\epsilon}{m_p^{k+1}} \sum_{x_q^{k+1} \in B_\epsilon(x_p^{k+1})} m_q W_q^{k+1} \tag{11}$$

$$m_p^{k+1} = \sum_{x_q^{k+1} \in B_\epsilon(x_p^{k+1})} m_q \tag{12}$$

where $B_\epsilon(x_p^{k+1})$ is a ^{n}dimensional sphere of radius ϵ centered at x_p^{k+1}. The particles which lie under this sphere are known as the ϵ-neighborhood of the material point (see [29]). This concept is conveniently sketched in Figure 1. Other parameters are the mass of the neighborhood m_p^{k+1}, the current free-energy density per unit mass W_q^{k+1} and the normalizing constant C_ϵ, which also defines the ϵ-neighborhood size, being $\epsilon = C_\epsilon h$.

The failure criterion consist of considering that a material point is failed when G_p^{k+1} surpasses the critical energy release rate that measures the material-specific energy, G_F. The convergence of this approach has been analyzed by Schmidt *et al.* (2009)[28], who proved that G_F converges to the Griffith fracture when the discretization size tends to zero. It is necessary to point out that, when a material point overpass the critical energy, its contribution to the internal forces vector is set to zero, but its contribution to the mass matrix is preserved.

As can be noticed, the eigenerosion algorithm relies over an energetic failure criterion. Because of this, unrealistic stress concentration (higher than tensile strength) appears in quasi-brittle materials [31]. To overcome this limitation, the aforementioned authors proposed the concept of eigensoftening to take into account the gradual failure in quasi-brittle materials. The
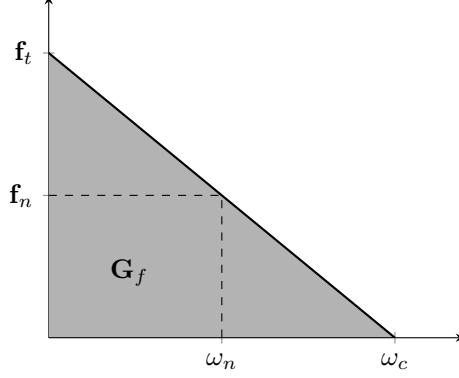
Figure 2: Scheme of a linear cohesive law, where the shaded area is G_f, f_t is the tensile strength, and w_c is the critical opening displacement.

idea behind this concept is inspired in the cohesive fracture. This gradual failure criterion is plotted in figure , where a linear decreasing cohesive law is presented to illustrate the concept earlier described. In the picture, the shaded region represents the static fracture energy per unit of area, G_F. Notice how a cohesive crack appears when the maximum tensile strength, f_t, is reached. Once the crack, w_n, reaches the value of the critical crack opening, w_c, a stress-free crack is attained. For intermediate values a damage value between zero and one represents the extension to which the material has failed. For the eigensoftening algorithm, a strength criterion for crack initialization was adopted. Particularly the maximum principal stress theory for brittle fracture was considered by authors [31]. With that purpose, the variation of the averaged strain energy density in the ϵ-neighborhood of the material point $\vec{x}_p^{k+1}$ can be obtained as

$$\delta W_{\epsilon,p} = \frac{\partial G_p}{C_\epsilon} = \frac{1}{m_p} \sum_{x_q^{k+1} \in B_\epsilon(x_p^{k+1})} m_q \sigma_{q,I} \delta\varepsilon_q, \tag{13}$$

where $\sigma_{q,I}$ is the maximum principal stress of each material point in the ϵ-neighborhood. At this point, an *effective* strain ε_q is introduced in order to obtain the variation of the local strain energy as $\delta W_q = \sigma_{q,1}\delta\varepsilon_q$. Now, with the assumption that the effective strain of each material point at every time step is constant in the neighborhood of $\vec{x}_p^{k+1}$, the equation (13) can be simplified to

$$\delta W_{\epsilon,p} = \frac{\delta\epsilon_p}{m_p} \sum_{x_q^{k+1} \in B_\epsilon(x_p^{k+1})} m_q \sigma_{q,I}. \tag{14}$$

9

Consequently, it is possible to define an equivalent critical stress at the material point $\vec{x}_p^{k+1}$ as

$$\sigma_{\epsilon,p} = \frac{1}{m_p} \sum_{x_q^{k+1} \in B_\epsilon(x_p^{k+1})} m_q \sigma_{q,I}, \qquad (15)$$

where m_p is the total mass of the ϵ-neighborhood, defined similarly than in the eigenerosion methodology (Eq. (12)). This definition of the equivalent critical stress leads to a definition of the averaged strain energy in terms of the averaged strain as $\delta W_{\epsilon,p} = \sigma_{\epsilon,p}\,\delta\varepsilon_p$. The softening behaviour is activated once $\sigma_{\epsilon,p}^{k+1}$ surpasses the tensile strength, f_t. This consists of a reduction of the internal forces as,

$$f_I^{int} = \sum_p (1 - \chi_p)\,\sigma_p^{k+1} \cdot grad(N_{Ip})\,\Omega_p \qquad (16)$$

where χ_p and Ω_p are respectively the damage or softening variable and the volume for each material point p. χ_p is any function, taking values between zero (an intact material) and one (completely failed material points), that relates the crack opening and the residual strength. To calculate it, typical shapes of cohesive laws such as linear, bilinear or exponential, may be employed. For the case of a linear softening such the sketched one in the Figure 2.3, χ_p is computed as,

$$1 - \chi = \frac{f_n}{f_t} = 1 - \frac{w_n}{w_c} \;\to\; \chi = \frac{w_n}{w_c}. \qquad (17)$$

Analogous to the crack band model presented by Bazant [33], Navas *et al.* [39] [31] introduced a band width parameter h_ϵ in order to relate the crack opening with the strain. Concerning this parameter, a typical value between two and four times the maximum size of the aggregates is adopted in the case of concrete as brittle material. The effective fracture strain $\varepsilon_{\epsilon,f}$ is defined as the difference between the strain at crack initialization, $\varepsilon_1(\vec{x}_p^0)$, and the current strain, $\varepsilon_1(\vec{x}_p^{k+1})$, for a material point p. Also, $\varepsilon_{\epsilon,f}$ can be represented as the current crack opening w_n within the band width, h_ϵ. Therefore,

$$\varepsilon_{\epsilon,f} = \varepsilon_1(\vec{x}_p^{k+1}) - \varepsilon_1(\vec{x}_p^0) = \frac{w_n}{h_\epsilon} \qquad (18)$$

Introducing (18) in (17), the damage variable can be computed as,

$$\chi = \frac{\varepsilon_{\epsilon,f}\,h^\epsilon}{w_c}. \qquad (19)$$

The function of χ presented in (19) represents a linear softening behaviour. For a general case, the damage variable can be expressed in terms of the following variables,

$$\chi = \chi(\varepsilon_{\epsilon,f}, h^\epsilon, f_t, w_c, G_f) \tag{20}$$

Implementation details can be consulted in Appendix B.

2.4. ϵ-neighborhood reconstruction : A node-linked method

The construction of the ϵ-neighborhood is a major issue of the proposed methodology. Since this operation could be extremely demanding, optimal numerical implementation should be employed. In opposite with the Cell-linked method proposed by Allen & Tildesley [40] where the definition of a numerical tolerance is required for auxiliar algorithms like Crossing Number [41] or Correct Even-Odd [42], the proposed methodology adopted herein is linked to the shape function neighbourhood. In order to avoid the aforementioned error prone techniques, we endeavour to exploit the meshfree benefits of the LME approximants to introduce a node-linked method. Due to the global definition of this interpolation technique, the classical interpretation of the FEM element typically adopted in MPM simulations is not required anymore. A linked list of tributary nodes is reconstructed with the closest node as starting point at each time step instead. Therefore, each node is assigned to an unique linked-list of those particles which are closest to it. This approach allows to reconstruct easily a search list with the support of the initial connectivity of the mesh and offers a suitable basis for an easy implementation of other interpolation techniques with minimum coding effort. A detailed explanation of the proposed algorithm can be found in Appendix C.

3. Cases of study and discussion

As noticed in [30], the EigenMPM have two important shortcomings. The first is the presence of stress instabilities even with GIMP shape functions. To overcome it, LME approximants are introduced as an alternative to the existing interpolation techniques. Its impressive performance mitigating spurious stress oscillations [43] under the MPM framework help to enhance notoriously the quality of the results as we can see in Section 3.1. Where both interpolation techniques are compared by carry out an eigenerosion simulation. The second limitation is concerning its inability to simulate properly quasi-brittle fracture [39]. It can be solved through the eigensoftening algorithm described in Section 2.3. A proof of it is exposed in Section ??, where experimental results of a drop-weight impact test are compared with those produced by eigensoftening computations.
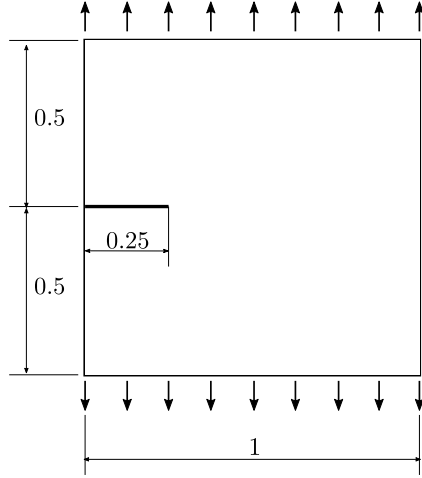
Figure 3: Geometry and boundary condition of the drop-weight impact test.

3.1. Edge-cracked square panel in mode I

This problem here presented is devoted to compare how much LME approximants are able to improve the result *versus* standard linear interpolation. It consists in a square plate of size $H = 1$ containing an initial edge crack of length $0.25 \cdot H$ loaded in a pure mode I by displacement control on the outer flanks of the plate, Figure 3. The constitutive model consider for numerical experiment is a linear-elastic Hookean material, where Young's modulus E = 1.06, the Poisson's ratio $\nu = 0.333$, and critical energy-release rate $G_F = 0.0001$. This set of parameters was taken from [29]. In MPM, two different discretization are required. In one hand a cartesian grid of nodes is consider with a nodal spacing value of 0.025. On the other hand, the plate will be modeled with a initial layout of four particles per element and occupying the Gauss quadrature positions.

Figure 4 clearly shows the presence of wiggles in both loading and fracture stages in the reaction-displacements curve when linear interpolation technique is used. In contrast, LME simulation does not exhibit these spurious oscillations and remains linear. Besides that, linear interpolation produces stiffer results than LME. This can be attributed to imprecision in the stress field due to grid-crossing phenomena.

On the other hand, Figure 5 exhibits more clearly the difference between linear interpolation and LME, since numerical instability becomes rather significant when particles crosses the boundary of the element in the linear case. Although this behavior does not affect significantly to the peak stress value in a hookean material [30], if hyperelastic materials are consider for
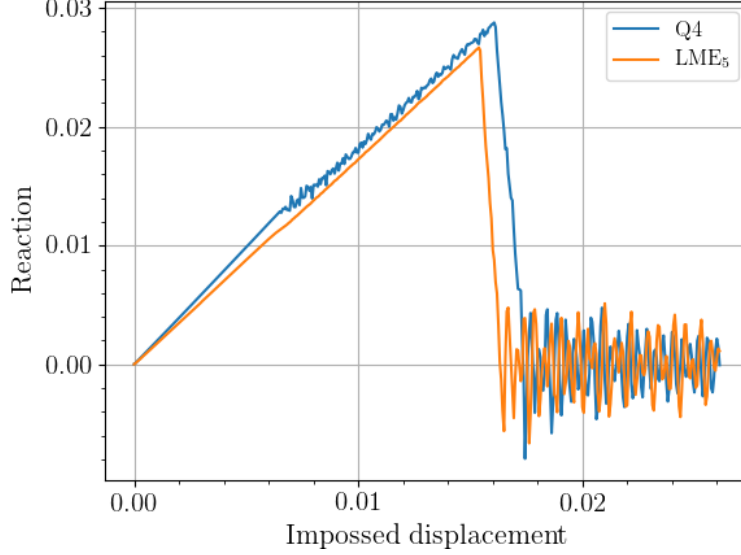
12

Figure 4: Evolution of the reaction forces plotted *versus* the imposed displacement for linear interpolation technique and the LME approximants.

future simulations, inaccuracies in the stress field could affect dramatically to the final result. On the other hand LME produces soft stress field evolution even after breaking. An important consideration regarding the presence of oscillations once both parts of the panel are separated, Figure 4. These phenomena should not be attributed to the eigenerosion algorithm since the fracture process is over. They are due to the dynamic nature of the solver.

3.2. Drop-weight impact test

Once the accuracy of the LME approximants have been proven in Section 3.1, henceforth will be adopted without comparing with linear interpolation. Therefore this section is devoted to proof the accuracy of the eigensoftening algorithm to simulate the behavior of quasi-brittle materials under dynamic loading. An example of this load case is the three-point bending test on a notched beam is conducted under impact loading. This kinds of experiments are challenging to reproduce numerically with an explicit solver since fracture occurs in a period of milliseconds and high strength materials are involved. Accordingly, really small time steps are required to achieve a simulation numerically stable. Additionally, this kind of simulations traditionally require the implementation of contact algorithm to reproduce the hammer impact in the beam. In the MPM, the implementation of this feature can be bypassed to obtain preliminary results. Nevertheless, this kind of algorithm could be

13
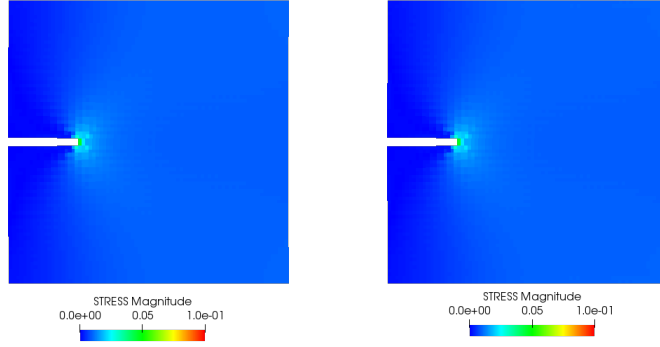
(a) t = 25
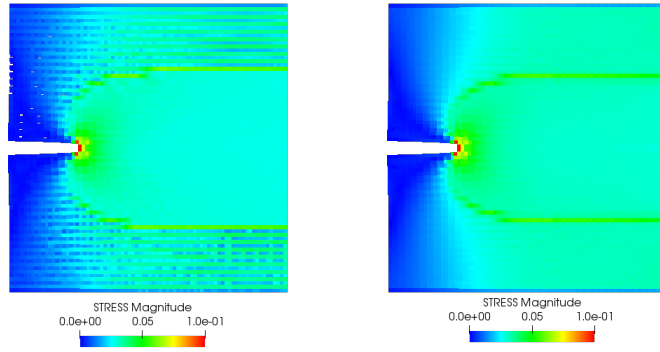
(b) t = 60
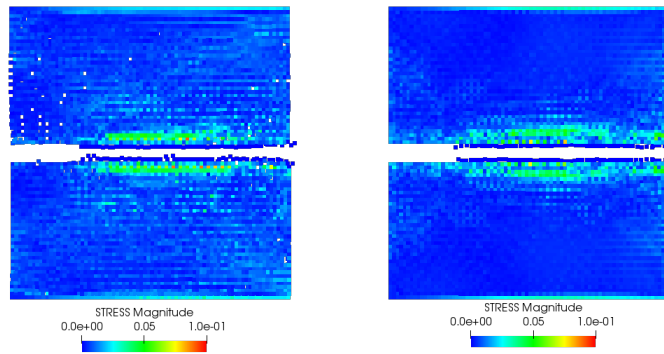
(c) t = 100

Figure 5: Evolution of the stress tensor magnitude for linear interpolation (pictures in the left side), and LME (pictures in the right side). Both simulations performed with an eigenerosion algorithm.
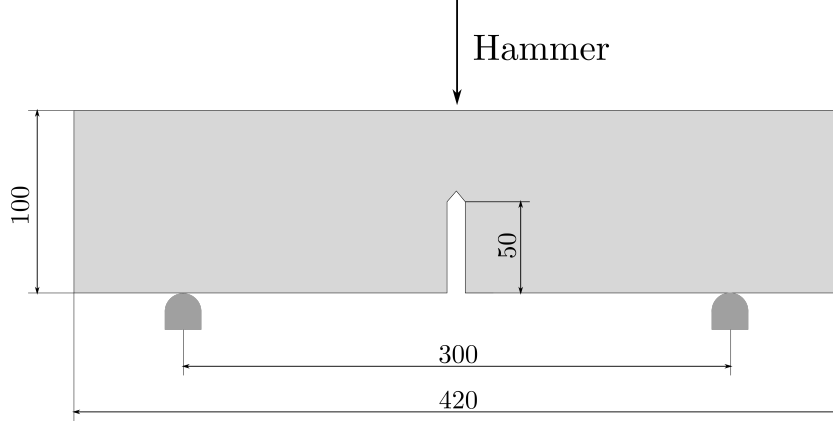
14

Figure 6: Geometry and boundary condition of the drop-weight impact test.

	ρ (kg/m^3)	f$_c$ (MPa)	f$_t$ (MPa)	G_F (N/m)	E (GPa)	d$_{max}$ (mm)
Value	2368	102.7	5.4	141	31	12

Table 1: Mechanical properties of the high strenght concrete.

implemented to get ever more accurate solutions. Although this is out of the scope of this document, future research of authors will overcome this limitation.

As in the study of Zhang *et al.* [44, 45], an impact hammer of 120.6 kg was employed to drop it at an impact speed of 881 mm/s. The beam dimensions where 100 mm x 100 mm (B x D) in cross section, and 420 mm in total lenght (L). The initial notch-depth ratio was approximately 0.5, and the span, S, was fixed at 300 mm during the tests, see Figure 6. The material adopted for the simulation was characterised by Navas *et al.* [31], and the material properties, such as the material density, ρ, the compressive strenght, f$_c$, the tensile strenght f$_t$, the specific fracture energy, G$_F$, and the elastic modulus E are given in table 1.

For the present research, a 2D setting of the experiment has been adopted. Both the hammer and the concrete beam are explicitly represented. Several levels of discretization were required to assess the objectiveness of the obtained results. The results here exposed are from a discretization of 30616 material points and 6297 nodes. To achieve better results, an unestructured grid layout has been adopted focusing the minimum nodal spacing, 0.47 mm, in the middle of the beam and in the impact surface of the hammer. For this
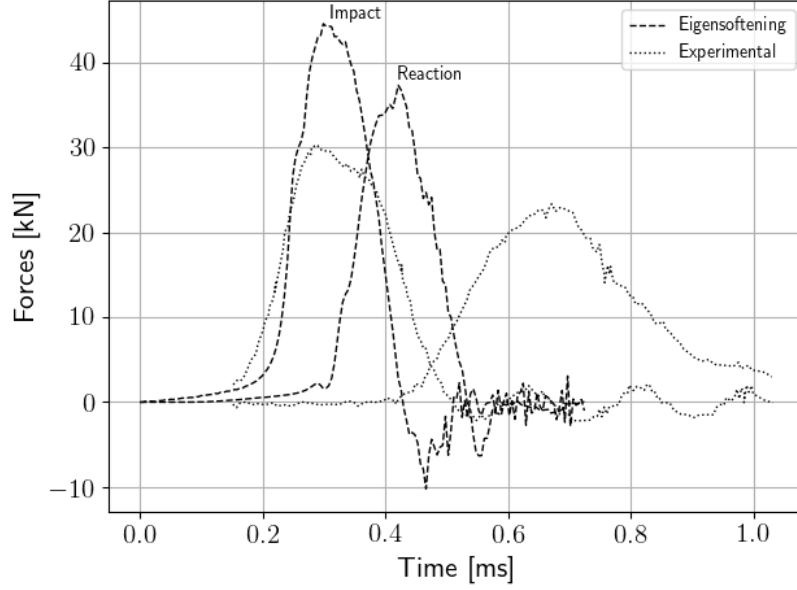
Figure 7: Evolution of the reaction forces plotted *versus* the imposed displacement for linear interpolation technique and the LME approximants.

simulation, $\widehat{\gamma}$ was fixed to 6.

First the reaction and impact forces are validated against their experimental counterparts. Since the impact forces applied by the hammer and the reaction forces at the two supports were experimentally measured, they are compared with numerical ones in Figure 7. Note that the general trend of both forces are correctly captured. Observe that in experimental solution the delay between impact peak and reactions peak does not agree with the numerical ones. On the other hand, if the delay is computed analytically through concrete wave speed is much closer to the numerical results. A feasible explanation to this unexpected result can due the composite nature of the concrete. Another discrepancy is in the much higher values of maximum impact and reaction forces in numerical than in experimental. In this case, this is a consequence of over-rigidity in the supports. Therefore, this results can be improved in future research by a suitable contact algorithm.

And finally horizontal stress distributions and crack propagation are extracted, see Figure 8. Stress evolution agrees with the results obtained by [31] under the OTM framework. Two additional considerations about this results are concerning the interpolation technique. In one hand, in the opposite to the uGIMP shape function, LME allows unstructured grids. This

16

is a remarkable benefit for this kind of simulations since the majority of the computational effort is clearly localised in a tiny region of the domain. And in the other hand there is the possibility to reduce the shape function support to avoid a material point in one side of the crack is affected by those in the other side of the crack.

4. Conclusions

Based on the EigenMPM approach to fracture proposed by Zhang *et al.* [30], we have proposed two addition improvements which solves the shortcomings presented in the original concept. First by bring to the MPM framework the concept of eigensoftening, which allow to consider gradual failure process of each material point. This concept can be compared with a cohesive law in the context of cohesive fracture. Furthermore, more elaborated damage curves can be designed to describe the failure process in more sophisticated materials. In this direction, an interesting future improvement of the algorithm would be the ability to simulate of crack patterns in composite material such carbon fiber. This leads a challenging research topic. Secondly, LME is employed to remove from the solution those wiggles due to inaccuracies in the stress integration. This interpolation technique could help to improve results in fracture propagation by adapting it through the deformation gradient. *A priori* this will enhance the already impressive localisation properties of eigensoftening and eigenerosion algorithms.
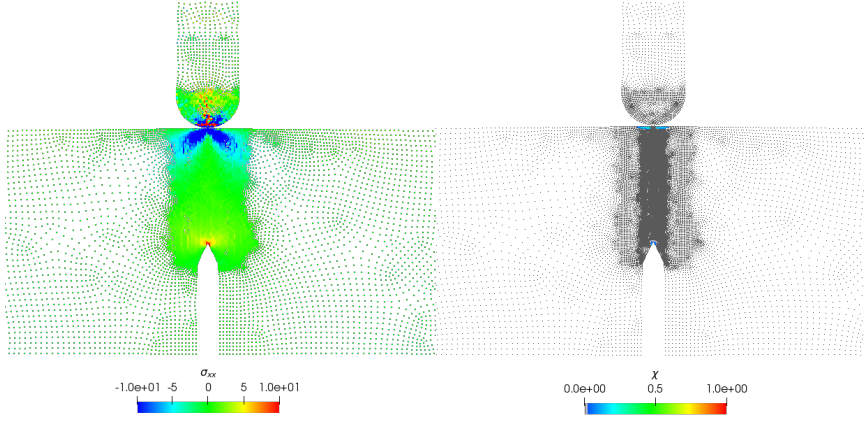
(a) t = 0.27 ms
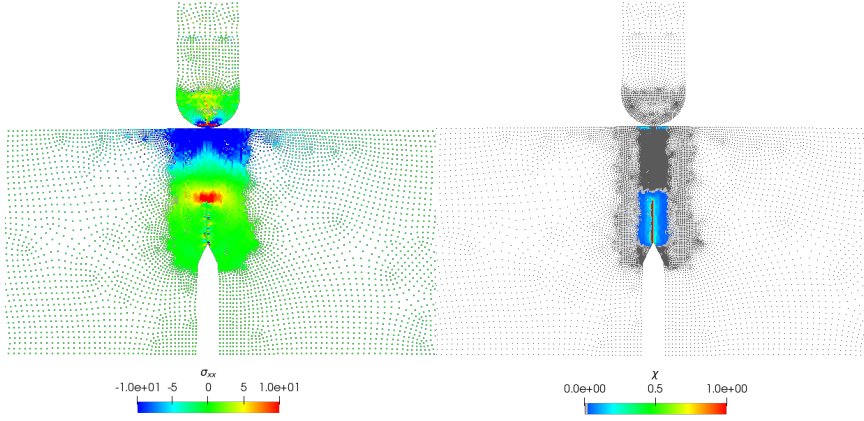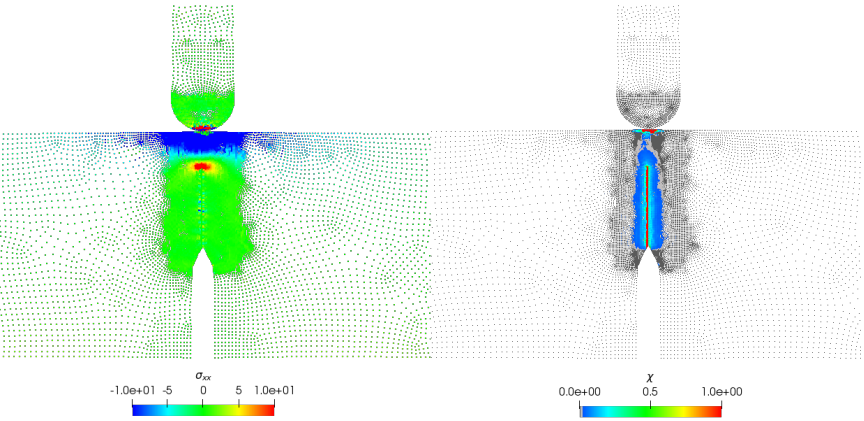

(b) t = 0.36 ms

(c) t = 0.45 ms

Figure 8: Evolution of the stress tensor magnitude for linear interpolation (pictures in the left side), and LME (pictures in the right side). Both simulations performed with an eigenerosion algorithm.

18

Appendix A. Explicit Newmark Predictor-Corrector algorithm

---

1 Update mass matrix : $\mathbf{m}_I = N_{Ip}^k \, m_p$

2 Explicit Newmark Predictor :

$$\vec{v}_I^{pred} = \frac{N_{Ip}^k m_p (\vec{v}_p^k + (1 - \gamma) \, \Delta t \, \vec{a}_p^k)}{m_I}$$

3 Impose essential boundary conditions : At the fixed boundary, set $\vec{v}_I^{pred} = 0$.

4 Deformation tensor increment calculation :

$$\Delta \varepsilon_p^{k+1} = \Delta t \, \dot{\varepsilon_p}^{k+1} = \Delta t \, \left[\vec{v}_I^{pred} \otimes grad(N_{Ip}^{k+1}) \right]^s$$

5 Update the density field : $\rho_p^{k+1} = \frac{\rho_p^k}{1 + tra\left[\Delta \varepsilon_p^{k+1} \right]}$.

6 Compute stress field and update damage parameter

7 Balance of forces calculation : Calculate the total grid nodal force $\vec{f}_I^{k+1} = \vec{f}_I^{int,k+1} + \vec{f}_I^{ext,k+1}$.

8 Explicit Newmark Corrector :

$$\vec{v}_I^{k+1} = \vec{v}_I^{pred} + \gamma \, \Delta t \, \frac{\vec{f}_I^{k+1}}{\mathbf{m}_I^{k+1}}$$

9 Update particles lagrangian quantities :

$$\vec{a}_p^{k+1} = \frac{N_{Ip}^k \vec{f}_I^k}{\mathbf{m}_I^k}$$

$$\vec{v}_p^{k+1} = \vec{v}_p^n + \Delta t \, \frac{N_{Ip}^k \, \vec{f}_I^k}{\mathbf{m}_I^k}$$

$$\vec{x}_p^{k+1} = \vec{x}_p^n + \Delta t \, N_{Ip}^k \, \vec{v}_I^k + \frac{1}{2} \Delta t^2 \, \frac{N_{Ip}^k \, \vec{f}_I^k}{\mathbf{m}_I^k}$$

10 Reset nodal values

Algorithm 1: Explicit Newmark Predictor-Corrector scheme

Appendix B. Eigensoftening Algorithm

Input: For each p, ϵ-neighbourhood, $f_{t,p}$, $h_{\epsilon,p}$, w_c
Output: Return damage parameter $\chi := \{\chi_p\}$

1   $\chi_p \leftarrow \chi_p^k$
2   **for** p *to* N_p **do**
3   **if** $\chi_p = 0$ $\epsilon_{f,p} = 0$ **then**
4   **for** $q \in B_{\epsilon,p}$ **do**
5         $\sigma_{q,I} \leftarrow \text{getEigenvaluesOf}(\sigma_q)$
6   **if** $\chi_q < 1$ **then**
7           $\sum m_p \sigma_{p,I} \leftarrow \sum m_p \sigma_{p,I} + m_q \sigma_{q,I}$
8   **end**
9         $m_p \leftarrow m_p + m_q$
10   **end**
11       $\sigma_{p,\epsilon} \leftarrow \frac{1}{m_p} \sum m_p \sigma_{p,I}$
12   **if** $\sigma_{p,\epsilon} > f_{t,p}$ **then**
13         $\epsilon_{f,p} = \epsilon_{I,p}$
14   **end**
15   **else if** $\chi_p \neq 1$ $\epsilon_{f,p} > 0$ **then**
16         $\chi_p^{k+1} \leftarrow \min\left\{1, \max\{\chi_p^k, \frac{(\epsilon_{I,p} - \epsilon_{f,p}) \, h_{\epsilon,p}}{w_c}\}\right\}$
17   **end**
18   **end**
19   **end**

Algorithm 2: Compute damage parameter χ_p^{k+1}

21

Appendix C. Node-linked method for ϵ-neighborhood reconstruction

Input: I_0 : Closest node for each particle
Input: I_{Nodes} : List of nodes close to each node
Input: $Particles_I$: List of particles close to each node
Output: neighborhood$_\epsilon$: ϵ-neighborhood for each particle

```
1  for p to Np do
2  |   For each p get I0
3  |   Eval INodes(I0)
4  |   for k ∈ INodes(I0) do
5  |   |   neighborhoodε^{k+1} = neighborhoodε^k ∪ ParticlesI(k)
6  |   end
7  |   for pε ∈ neighborhoodε do
8  |   |   if distance(pε, p) > ε then
9  |   |   |   pop pε from neighborhoodε
10 |   |   end
11 |   end
12 end
```

Algorithm 3: ϵ-neighborhood reconstruction algorithm

References

[1] G. Barenblatt, The mathematical theory of equilibrium cracks in brittle fracture., Advances in Applied Mechanics 7 (1962) 55–129.

[2] A. Hillerborg, M. Modéer, P. Petersson, Analysis of crack formation and crack growth in concrete by means of fracture mechanics and finite elements., Cement and Concrete Research. 6 (1976) 773–782.

[3] M. Ortiz, A. Pandolfi, Finite-deformation irreversible cohesive elements for three-dimensional crack-propagation analysis., International Journal for Numerical Methods in Engineering. 44 (1999) 1267–1282.

[4] A. Pandolfi, M. Ortiz, An efficient adaptive procedure for three-dimensional fragmentation simulations., Engineering with Computers. 18(2) (2002) 148–159.

[5] G. Ruiz, M. Ortiz, A. Pandolfi, Three-dimensional finite-element simulation of the dynamic Brazilian tests on concrete cylinders, International Journal for Numerical Methods in Engineering 48 (2000) 963–994.

[6] T. Belytschko, H. Chen, J. Xu, G. Zi, Dynamic crack propagation based on loss of hyperbolicity and a new discontinuous enrichment., International Journal for Numerical Methods in Engineering. 58 (2003) 1873–1905.

[7]

[8] Z. Chen, W. Hu, L. Shen, X. An, R. Brannon, An evaluation of the mpm for simulating dynamic failure with damage diffusion, Engineering Fracture Mechanics 69 (2002) 1873–1890. `doi:10.1016/S0013-7944(02)00066-8`.

[9] J. Nairn, Material point method calculations with explicit cracks, Computer Modeling in Engineering & Sciences 4 (6) (2003) 649–664. `doi:10.3970/cmes.2003.004.649`.
URL `http://www.techscience.com/CMES/v4n6/33290`

[10] Z. Chen, L. Shen, Y.-W. Mai, Y.-G. Shen, A bifurcation-based decohesion model for simulating the transition from localization to decohesion with the mpm, Zeitschrift fur Angewandte Mathematik und Physik 56 (2005) 908–930. `doi:10.1007/s00033-005-3011-0`.

[11] T. Belytschko, Y. Lu, L. Gu, M. Tabbara, Element-free galerkin methods for static and dynamic fracture, International Journal of Solids and Structures 32 (17) (1995) 2547 – 2570. `doi:https://doi.org/10.1016/0020-7683(94)00282-2`.
URL `http://www.sciencedirect.com/science/article/pii/0020768394002822`

[12] T. Belytschko, D. Organ, C. Gerlach, Element-free galerkin methods for dynamic fracture in concrete, Computer Methods in Applied Mechanics and Engineering 187 (3) (2000) 385 – 399. `doi:https://doi.org/10.1016/S0045-7825(00)80002-X`.
URL `http://www.sciencedirect.com/science/article/pii/S004578250080002X`

[13] X. Zhuang, C. Augarde, K. Mathisen, Fracture modeling using meshless methods and level sets in 3d: Framework and modeling, International Journal for Numerical Methods in Engineering 92 (2012) 969–998. `doi:10.1002/nme.4365`.

[14] N. Muthu, S. Maiti, B. Falzon, I. Guiamatsia, A comparison of stress intensity factors obtained through crack closure integral and other ap-

23

proaches using extended element-free galerkin method, Computational Mechanics 52. `doi:10.1007/s00466-013-0834-y`.

[15] Y. Wang, H. T. Tran, G. D. Nguyen, P. G. Ranjith, H. H. Bui, Simulation of mixed-mode fracture using sph particles with an embedded fracture process zone, International Journal for Numerical and Analytical Methods in Geomechanics n/a (n/a). `arXiv:` `https://onlinelibrary.wiley.com/doi/pdf/10.1002/nag.3069`, `doi:10.1002/nag.3069`.
URL `https://onlinelibrary.wiley.com/doi/abs/10.1002/nag.` `3069`

[16] Y. Wang, H. Bui, G. Nguyen, P. Ranjith, A new sph-based continuum framework with an embedded fracture process zone for modelling rock fracture, International Journal of Solids and Structures 159 (2019) 40–57. `doi:10.1016/j.ijsolstr.2018.09.019`.

[17] B. Li, F. Habbal, M. Ortiz, Optimal transportation meshfree approximation schemes for fluid and plastic flows, International Journal for Numerical Methods in Engineering 83 (12) (2010) 1541–1579. `doi:` `10.1002/nme.2869`.
URL `http://doi.wiley.com/10.1002/nme.2869`

[18] B. Li, A. Kadane, G. Ravichandran, M. Ortiz, Verification and validation of the optimal-transportation meshfree (otm) simulation of terminal ballistics., International Journal for Impact Engineering 42 (2012) 25–36.

[19] A. Pandolfi, B. Li, M. Ortiz, Modeling fracture by material-point erosion., International Journal of fracture 184 (2013) 3–16.

[20] B. Li, A. Pandolfi, M. Ortiz, Material-point erosion simulation of dynamic fragmentation of metals., Mechanics of Materials 80 (2015) 288–297.

[21] Y. D. Ha, F. Bobaru, Characteristics of dynamic brittle fracture captured with peridynamics, Engineering Fracture Mechanics 78 (6) (2011) 1156 – 1168. `doi:https://doi.org/10.1016/j.engfracmech.` `2010.11.020`.
URL `http://www.sciencedirect.com/science/article/pii/` `S0013794410004959`

[22] T. Rabczuk, H. Ren, A peridynamics formulation for quasi-static fracture and contact in rock, Engineering Geology 225

(2017) 42 – 48, special Issue: Characterisation of Fractures in Rock: from Theory to Practice (ROCKFRAC). doi:https://doi.org/10.1016/j.enggeo.2017.05.001.

375 URL http://www.sciencedirect.com/science/article/pii/S0013795217306907

[23] Y. GUO, J. Nairn, Three-dimensional dynamic fracture analysis using the material point method, Computer Modeling in Engineering Sciences 16.

380 [24] H. Tan, J. Nairn, Hierarchical, adaptive, material point method for dynamic energy release rate calculations, Computer Methods in Applied Mechanics and Engineering 191 (2002) 2123–2137. doi:10.1016/S0045-7825(01)00377-2.

[25] Y. GUO, J. Nairn, Calculation of j-integral and stress intensity factors using the material point method, CMES. Computer Modeling in Engineering Sciences 6.

385

[26] Z. Chen, R. Feng, X. An, L. Shen, A computational model for impact failure with shearinduced dilatancy, International Journal for Numerical Methods in Engineering 56 (2003) 1979 – 1997. doi:10.1002/nme.651.

390 [27] S. DL, L. Schreyer, Mpm simulation of dynamic material failure with a decohesion constitutive model, European Journal of Mechanics - A/Solids 23 (2004) 423–445. doi:10.1016/j.euromechsol.2004.02.007.

[28] B. Schmidt, F. Fraternali, M. Ortiz, Eigenfracture: an eigendeformation approach to variational fracture., SIAM J. Multiscale Model. Simul. 7 (2009) 1237–1266.

395

[29] A. Pandolfi, M. Ortiz, An eigenerosion approach to brittle fracture., International Journal for Numerical Methods in Engineering 92 (2012) 694–714.

400 [30] K. Zhang, S.-L. Shen, A. Zhou, Dynamic brittle fracture with eigenerosion enhanced material point method, International Journal for Numerical Methods in Engineering n/a (n/a). arXiv:https://onlinelibrary.wiley.com/doi/pdf/10.1002/nme.6381, doi:10.1002/nme.6381.

405 URL https://onlinelibrary.wiley.com/doi/abs/10.1002/nme.6381

25

[31] P. Navas, R. Yu, B. Li, G. Ruiz, Modeling the dynamic fracture in concrete: an eigensoftening meshfree approach, International Journal of Impact Engineering 113. `doi:10.1016/j.ijimpeng.2017.11.004`.

[32] P. Navas, S. López-Querol, R. C. Yu, M. Pastor, Optimal transportation meshfree method in geotechnical engineering problems under large deformation regime, International Journal for Numerical Methods in Engineering`doi:10.1002/nme.5841`.

[33] Z. Bažant, B. Oh, Crack band theory for fracture in concrete., Materials and Structures. 16 (1983) 155–177.

[34] M. Molinos, P. Navas, M. Pastor, M. Martín Stickle, On the dynamic assessment of the Local-Maximum Entropy Material Point Method through an Explicit Predictor-Corrector Scheme, Computer Methods in Applied Mechanics and Engineering Under review (2020) –.

[35] M. Arroyo, M. Ortiz, Local maximum-entropy approximation schemes: A seamless bridge between finite elements and meshfree methods, International Journal for Numerical Methods in Engineering`doi:10.1002/nme.1534`.

[36] D. L. Sulsky, H. Schreyer, Z. Chen, A particle method for history-dependent materials, Computer Methods in Applied Mechanics and Engineering 118 (1) (1994) 179–196. `doi:10.1016/0045-7825(94)90112-0`.

[37] E. Jaynes, Information Theory and Statistical Mechanics, The Physical Review 106 (4) (1957) 620–630.

[38] C. E. Shannon, A Mathematical Theory of Communication, Bell System Technical Journal`doi:10.1002/j.1538-7305.1948.tb01338.x`.

[39] P. Navas, R. Yu, G. Ruiz, Meshfree modeling of the dynamic mixed-mode fracture in frc through an eigensoftening approach, Engineering Structures 172. `doi:10.1016/j.engstruct.2018.06.010`.

[40] M. P. Allen, D. J. Tildesley, Computer Simulation of Liquids, Clarendon Press, USA, 1989.

[41] M. Shimrat, Algorithm 112: Position of point relative to polygon, Commun. ACM 5 (8) (1962) 434. `doi:10.1145/368637.368653`.
URL `https://doi.org/10.1145/368637.368653`

[42] M. Galetzka, P. Glauner, A simple and correct even-odd algorithm for the point-in-polygon problem for complex polygons, 2017. `doi: 10.5220/0006040801750178`.

[43] E. Wobbes, R. Tielen, M. Möller, C. Vuik, Comparison and unification of material-point and optimal transportation meshfree methods, Computational Particle Mechanics`doi:10.1007/s40571-020-00316-7`.

[44] X. Zhang, G. Ruiz, R. Yu, M. Tarifa, Fracture behaviour of high-strength concrete at a wide range of loading rates., International Journal of Impact Engineering 36 (2009) 1204–1209.

[45] X. Zhang, R. Yu, G. Ruiz, M. Tarifa, M. Camara, Effect of loading rate on crack velocities in hsc., International Journal of Impact Engineering 37 (2010) 359–370.